ACS Photonics

Article

pubs.acs.org/journal/apchd5

# Superconductivity-Induced Transparency in Terahertz Metamaterials

Odeta Limaj,*[,†,⊗] Flavio Giorgianni,[†] Alessandra Di Gaspare,[‡] Valeria Giliberti,[‡,§] Gianluca de Marzi,[⊥] Pascale Roy,[∥] Michele Ortolani,[§] Xiaoxing Xi,[△] Daniel Cunnane,[△] and Stefano Lupi[#]

[†]INFN and Department of Physics, Sapienza University of Rome, Rome, Italy

[‡]CNR Istituto di Fotonica e Nanotecnologie (IFN), Rome, Italy

[§]Department of Physics, Sapienza University of Rome, Rome, Italy

[⊥]ENEA, Frascati Research Centre, Frascati, Italy

[∥]Synchrotron SOLEIL, Gif-sur-Yvette, France

[△]Department of Physics, Temple University, Philadelphia, Pennsylvania 19122, United States

[#]INFN and Department of Physics, Sapienza University of Rome, Rome, Italy

[⊗]Insititute of Bioengineering, École polytechnique fédérale de Lausanne (EPFL), Lausanne, Switzerland

Supporting Information

**ABSTRACT:** A plasmonic analogue of electromagnetically induced transparency is activated and tuned in the terahertz (THz) range in asymmetric metamaterials fabricated from high critical temperature ($T_c$) superconductor thin films. The asymmetric design provides a near-field coupling between a superradiant and a subradiant plasmonic mode, which has been widely tuned through superconductivity and monitored by Fourier transform infrared spectroscopy. The sharp transparency window that appears in the extinction spectrum exhibits a relative modulation up to 50% activated by temperature change. The interplay between ohmic and radiative damping, which can be independently tuned and controlled, allows for engineering the electromagnetically induced transparency of the metamaterial far beyond the current state-of-the-art, which relies on standard metals or low-$T_c$ superconductors.

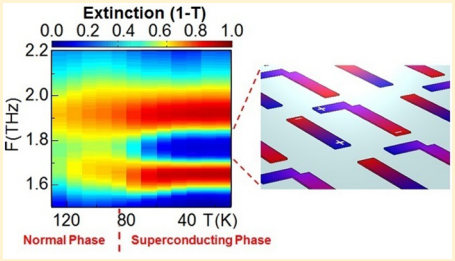


**KEYWORDS:** *superconductivity, electromagnetic-induced transparency, THz, dark mode, Fano resonance, tunable metamaterials*

Electromagnetically induced transparency (EIT) is a quantum interference effect that permits light propagation in an otherwise opaque medium. It was first observed in a three-state lead-vapor system where the opening of a narrow transparency window in a broad absorption spectrum was ascribed to destructive interference between two possible excitation pathways in the system.[1] The dramatic effects of EIT on the dispersive properties of the medium may allow for photon slowdown or storage and optical data buffering.[2−4] A plasmonic analogue of EIT has been recently demonstrated in planar fishnet metamaterials, coupled resonators, and waveguides[5−13] from the millimeter[14,15] to infrared[16,17] up to the visible range.[18] In these examples of EIT plasmonic analogues a bright superradiant mode with a quasi-continuum spectrum provides the dipole-allowed transition in the corresponding atomic picture, while a dark subradiant mode represents the dipole-forbidden excitation (metastable state).[19] In the specific case of plasmonic EIT, the discrete dark mode has a plasmonic nature; however, depending on the phenomen, it can also be either a molecular vibration (as in surface-enhanced infrared absorption spectroscopy[20]), a diffraction order,[21] or phonon excitation.[22]

Nevertheless, in the aforementioned works the EIT transparency window is set by the geometrical parameters or material properties, with no possibility for active control of the optical response. Some recent works have explored the options for active control of EIT response through optical pulses,[12] superconductivity,[23−26] and mechanic stress on compliant substrates.[28] However, in these works no insight was put into the coupling regime of the specific plasmonic modes, which is the key mechanism defining the EIT response. In fact, the coupling regime between the plasmonic modes involved in the interference mechanism rules the interplay between electromagnetically induced transparency and absorption (EIA).[29] Within a coupled harmonic oscillators approach, ohmic and radiative damping are key mechanisms controlling the EIT/EIA regime (as extensively discussed in ref 29); therefore a comprehensive investigation of EIT tunability in plasmonic nanostructures cannot disregard damping mechanisms.

In this work we present a proof-of-concept platform offering both EIT tuning and independent control over ohmic and radiative losses. In the terahertz (THz) range superconductivity is a unique tool for such a purpose, since it allows for continuously tuning the optical properties and ohmic damping of the plasmonic medium through an external input such as an electric or magnetic field, current, or temperature. In the THz

**Received:** November 19, 2013
**Published:** June 13, 2014

  

range, the superconducting transition driven by these external inputs affects the electrodynamic properties of superconductors in a range of about 4−6 Δ (with Δ the superconducting energy gap), matching the entire THz spectral region.[7] In this spectral range ohmic losses are (in principle) absent, and the gap opens within a few degrees below the critical temperature $T_c$, thus providing a fine control over the plasmonic response by superconductivity.[14,26,27,30,31] In this framework, high critical temperature cuprate superconductors (HTCS) are of particular interest for two reasons: (i) they exhibit a $T_c$ up to 140 K, hence well above liquid nitrogen temperature (77 K), which makes them very convenient for technological applications; (ii) although losses never reach zero due to nodal points of the gap in the momentum space (due to the d-wave symmetry of the gap function) HTCS provide a much broader frequency ($\omega$) range of tunability, extending beyond 10 THz compared to conventional Bardeen−Cooper−Schrieffer (BCS) superconductors.[32,33]

The exceptional potential of superconductivity finds a limitation in THz plasmonics due to the fact that ohmic losses reduction at these frequencies is not as effective as at optical frequencies. Indeed, the high absolute value of the real part of electrical permittivity of metals at these frequencies makes them almost perfect conductors. Consequently, the role of other damping mechanisms, such as radiative ones, becomes of crucial importance. In this work we have implemented plasmonic devices in which we engineer radiative losses through near-field interaction between a bright and a dark plasmonic mode. The ohmic damping is continuously tuned through superconductivity, resulting in a modulation of the electromagnetic transparency. The temperature-controlled relative modulation of the extinction coefficient across the superconducting transition reaches 50% of the off-state value, corresponding to a dark mode resonance with a quality factor of about 13.

## RESULTS AND DISCUSSION

The proposed EIT device is based on an asymmetric plasmonic structure[16] made of high temperature superconductor $YBa_2Cu_3O_{7-\delta}$ (YBCO, $T_c$ = 83 K). Nanofabrication was performed using electron beam lithography (EBL) on commercial 200 nm thick YBCO films (THEVA, Germany) grown on a 500 $\mu$m thick sapphire substrate. Wet etching in 0.075% nitric acid for 1 min allowed for selective YBCO removal. The plasmonic rectangular array had a pitch of $p_x$ = 40 $\mu$m and $p_y$ = 48 $\mu$m, along $x$ and $y$, respectively. Each resonator element of the array is constituted by a pair of rods of length $D$ = 28 $\mu$m and width $W$ = 5 $\mu$m (see inset of Figure 1c). The unit cell can support a bright and a dark excitation for an electric field polarized parallel to the $y$ axis (see insets in Figure 1b and c). The bright mode has a dipolar nature and can directly couple to normal incident radiation when the radiation electric field is polarized along the rod length, while the dark mode cannot be excited in the same condition due to its symmetry (quadrupolar) bearing no net electric dipole. When the $x$-axis symmetry is broken by the addition of a horizontal arm, a near-field interaction between bright and dark mode is activated. The interaction strength is controlled by the horizontal arm length $S$, which measures the asymmetry of the structure. By geometric tuning through $S$, different coupling regimes have been engineered varying the coupling strength from zero to maximum allowed by design (see Figure 1). The three samples have been denoted as $S_0$ ($S$ = 0 $\mu$m), $S_6$ ($S$ = 6.5 $\mu$m), and $S_{13}$ ($S$ = 13.5 $\mu$m). Finite difference time domain (FDTD) electromagnetic simulations have been performed using the software CST Microwave Studio Suite in order to calculate the scattering parameters and the electric field profiles of the plasmonic excitations supported by the structure. The geometrical parameters of the patterns are set to make the resonant features lie in the 1−3 THz range, i.e., inside the frequency range where we expect a strong modulation of YBCO optical properties at the onset of the superconducting state.

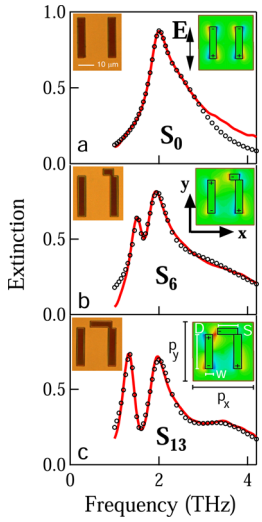


**Figure 1.** Experimental extinction coefficient (red curves) and fit (black circles) for the $S_0$ (a), $S_6$ (b), and $S_{13}$ (c) samples at $T$ = 6 K. The geometrical parameters, as reported in the schematic drawing in panel c, are $D$ = 28 $\mu$m, $W$ = 5 $\mu$m, $p_x$ = 40 $\mu$m, and $p_y$ = 48 $\mu$m. In the insets in panel a−c: FDTD simulations profile for the $x$ component of the electric field in correspondence with the EIT window at $\omega$ = 1.8 THz. In the insets on the left the optical images of the fabricated samples are reported.

Fourier transform infrared (FT-IR) spectroscopy transmission measurements have been performed with a Bruker Michelson interferometer coupled to a closed-cycle cryogenerator and a 4.2 K silicon bolometer. The transmittance of the array ($T(\omega)$) was measured at normal incidence in the range 0.3−10 THz by the use of THz radiation collected from the AILES beamline at the synchrotron Soleil[39] and in a temperature range $T$ = 6−300 K using a bare sapphire substrate as reference. Notice that the extension to the THz range is greatly eased by the use of edge radiation.[40] A wire-grid polarizer was used to select the radiation component parallel to the long arm rod (see Figure 1b). The experimental extinction coefficient has been calculated from transmittance data as $E(\omega) = 1 - T(\omega)$. This quantity accounts for the radiation that has not been transmitted by the system due to absorption, reflection and scattering phenomena.[19,41,42] The extinction coefficient for the three samples at $T$ = 6 K is reported in Figure 1. The $S_0$ sample in panel a exhibits a broad absorption band centered around 2 THz typical of a dipole antenna response.[43] As the $x$-axis symmetry of the dipolar structure is broken by the addition of the horizontal arm in samples $S_6$ and $S_{13}$, a transparency window (i.e., $E(\omega) \approx 0$) opens at 1.8 THz close to the peak absorption of the dipolar band (panels b and c). This window becomes narrower and deeper as $S$-length increases, with a relative modulation of $E(\omega)$ of more than 70% for sample $S_{13}$ (panel c) with respect to $S_0$. Note that an additional peak appears around 3.7 THz when the symmetry of


dx.doi.org/10.1021/ph500104k | ACS Photonics 2014, 1, 570−575

the unit cell is broken: this mode has a quadrupolar symmetry and is associated with the second-order plasmonic excitation of the single rod antenna.[44]

Comparing with the FDTD simulations of the in-plane field pattern at 1.8 THz, reported in the insets of Figure 1, the transparency window can clearly be attributed to the field components with quadrupolar symmetry appearing close to the horizontal arm.

In order to highlight the role of superconductivity in the induced-transparency phenomenon, the optical response of the three samples was measured as a function of temperature $T$. In Figure 2 the extinction coefficient is reported for selected $T_s$ in the range 6−120 K. We start by describing the effect of the superconducting transition on the THz extinction spectra of the $S_0$ sample where only the bright mode is present. As seen in Figure 2a, as $T$ is lowered, a narrowing of the dipole absorption band associated with the bright mode is observed below $T_c$ and no transparency is induced. This line shape narrowing is related to a decrease of the imaginary part of the dielectric function (*i.e.*, of the ohmic losses) of YBCO as the film undergoes the superconducting transition.[32,33] The resonance frequency of the bright mode, $\omega_b$ (which has been determined through a Lorentzian fit; see below), exhibits a nonmonotonic dependence on temperature, with a maximum red-shift (about 3%) corresponding to $T \approx 75$ K (see the inset in Figure 2a). In particular, the softening of $\omega_b$ is caused by the divergence of the kinetic inductance, $L_k$, of the superconducting Cooper pairs, which start to form when $T$ approaches $T_c$ from above.[23] The $T$ value of maximum softening does not correspond to $T_c$, because it results from the combined effect of increasing superconducting carrier density and decreasing $L_k$ as $T$ is lowered further below $T_c$. This observation was already reported in ref 23 for YBCO split ring resonators (SRR), where, in a first approximation, one has $\omega_b = 1/\sqrt{(L_k + L_g)C}$, where $L_g$ and $C$ are the geometric inductance and capacitance, respectively. In the present case, the softening of the resonance due to the singularity at $T_c$ is much weaker than in SSR due to the smaller absolute value of $L_k$ with respect to $L_g$. Therefore, for a quantitive analysis of the induced transparency, we will consider in the following $\omega_b$ to be $T$-independent.

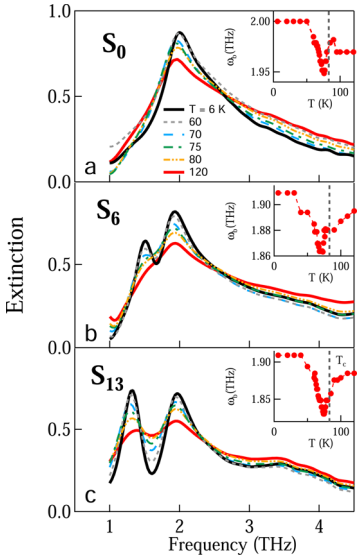


**Figure 2.** Extinction coefficient for selected temperatures between $T$ = 6 K and $T$ = 120 K for the $S_0$ (a), $S_6$ (b), and $S_{13}$ (c) samples for an electric field polarized along the rod antennas ($y$ axis of 1). The data for the lowest and highest temperature are described by solid lines, while intermediate temperatures are reported as different dashed lines. In the inset: Resonance frequency of the bright mode $\omega_b$ as a function of temperature. The values of $\omega_b$ have been extracted from the experimental data renormalized by the interference pattern $\sigma_a(\omega)$ obtained by the fit procedure in order to eliminate the (weak) frequency shift given by interaction with the dark mode (see text). Vertical dashed line in the inset denotes the critical temperature $T_c$ of YBCO (83 K).

We now turn to the transparency regime by considering sample $S_6$ in Figure 2b. It can be observed that the transparency window is strongly affected by temperature changes. It is very narrow for $T$ = 6 K, but it becomes broader for increasing $T$ until it is almost suppressed above $T_c$. The available modulation range is about 30% when changing $T$ from 6 to 77 K. This value is reduced to 15% for an increase of $T$ above liquid nitrogen temperature (77 to 100 K). The performance of the $S_{13}$ sample shown in Figure 2c has more potential for future applications. First of all, unlike the previous sample, the transparency modulation is already observed in the normal state, indicating that superconductivity is not a precondition for observing it. Moreover, the relative modulation of the extinction coefficient increased to 50% as $T$ is varied from 6 to 77 K and to 30% from 77 to 100 K.

The key mechanism for this wide range of tunability relies on YBCO's peculiar properties. The normal state dc conductivity of YBCO films at 100 K is $\sim 10^4\ \Omega^{-1}\ cm^{-1}$. At the onset of the superconducting state, it experiences an increase of the optical conductivity by more than a factor of 10 at 1.8 THz.[34] Furthermore, this behavior is observed in a wide frequency range extending well inside the THz range. Standard metals at these frequencies exhibit an almost perfect conductor behavior; therefore their ohmic damping can be weakly tuned through temperature. Even superconducting compounds with high values of optical conductivity ($10^5$−$10^6\ \Omega^{-1}\ cm^{-1}$ at 1.8 THz)[35−37] in the normal state prevent the full utilization of the tunability opportunities offered by superconductivity. To demonstrate that our YBCO-based plasmonic structure features the highest tunability performances with respect to other high-conductivity superconductors, we investigated the optical behavior of identical nanostructures fabricated on $MgB_2$ BCS superconducting films ($T_c$ = 39.4 K, detailed info on nanofabrication in the SI) with $10^6\ \Omega^{-1}\ cm^{-1}$ dc conductivity at 50 K.[38] As shown in Figure 3 the extinction coefficient for

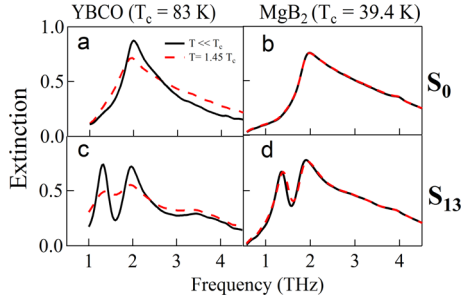


**Figure 3.** Extinction coefficient for YBCO (a, c) and $MgB_2$ (b, d) samples without ($S_0$) and with ($S_{13}$) EIT. The data for $T$ = 6 K (black) and $T = 1.45T_c$ (red) are reported. A remarkable modulation with temperature for the EIT transparency window is observed in both YBCO samples at ∼1.8−2 THz, while almost no variation is observable in the case of $MgB_2$.


dx.doi.org/10.1021/ph500104k | ACS Photonics 2014, 1, 570−575

$MgB_2$ samples exhibits almost no variation (Figure 3b, $S_0$) or extremely weak tunability (Figure 3d, $S_{13}$) upon varying the temperature from $T$ = 6 K up to 75 K (1.45$T_c$). It is important to mention that scaling the resonant response of the nanostructure at lower frequencies, to move deeper inside the superconducting gap of $MgB_2$ ($\Delta$ = 1.8 THz),[38] would bring in a stronger superconducting regime and consequently an improved tunability of the plasmonic response. However, the high conductivity of $MgB_2$ in the normal state puts an intrinsic limit on the tunability range of the device with superconductivity; furthermore it would not be accessible for high-frequency THz applications due to the relatively small superconducting gap of $MgB_2$.

The advantage provided by superconductivity for our YBCO plasmonic devices can be better appreciated from a quantitative analysis of the line shape parameters, which we performed through a best-fit procedure. The plasmonic line shape results from a Fano interference pattern where, in analogy with quantum EIT, two excited states are involved in the radiation absorption process. The first is a broad (superradiant) bright mode, which plays the role of the excited state $|b\rangle$ for the dipole-allowed transition. The second is a dark (subradiant) quadrupole mode[16] representing the metastable state $|d\rangle$. Through symmetry breaking by the addition of the horizontal arm of length $S$ (see Figure 1b and c), the bright and dark mode can couple in the near-field limit, resulting in a destructive interference between the two possible absorption pathways from the ground state $|0\rangle$: $|0\rangle \rightarrow |b\rangle$ and $|0\rangle \rightarrow |b\rangle \rightarrow |d\rangle \rightarrow |b\rangle$.[1]

In this scenario, the extinction coefficient can be described as the product of the extinction coefficient of the bright mode, $\sigma_b(\omega)$, and the Fano envelope function, $\sigma_a(\omega)$, representing the interference.[45] One can assume a Lorentzian form for the bright mode line shape:

$$\sigma_b(\omega) = \frac{A\Gamma\omega}{(\omega_b{}^2 - \omega^2)^2 + \Gamma^2\omega^2} \quad (1)$$

where $A$ is the resonance intensity, $\omega_b$ is the real part of the resonance frequency, and $\Gamma$ its imaginary part, accounting for both ohmic and radiative damping.[46] The Fano envelope function $\sigma_a$ can be written in the form[45]

$$\sigma_a(\omega) = \frac{\left(\frac{\omega^2 - \omega_a{}^2}{(\omega_a + W_a)^2 - \omega_a{}^2} + q\right)^2 + b}{\left(\frac{\omega^2 - \omega_a{}^2}{(\omega_a + W_a)^2 - \omega_a{}^2}\right)^2 + 1} \quad (2)$$

where $\omega_a$ is the frequency of maximum constructive interference, $W_a$ is an approximation of its spectral width valid for $W_a \ll \omega_a$, $q$ is the Fano asymmetry parameter, and $b$ is a damping parameter due to intrinsic losses of the dark (quadrupolar) resonance. The total extinction coefficient, $E(\omega) = \sigma_b(\omega)\,\sigma_a(\omega)$, is the measurable quantity to be compared with the experimental data. An additional Lorentzian line shape (assumed to be independent of $T$) has been added in the fit at high frequency to account for the single rod antenna quadrupolar excitation in the range 3−4 THz. In Figure 1 one sees that a good agreement is observed between the fitting curves (black circles) and the experimental data (red curves). The best-fit parameters of both the bright and dark resonances as a function of temperature have been extracted. The resonance parameters not explicitly written in the fitting equations are described in the Supporting Information.

In Figure 4a the damping $\Gamma$ of the bright mode is reported for the three samples. For all samples, $\Gamma$ exhibits a reduction by

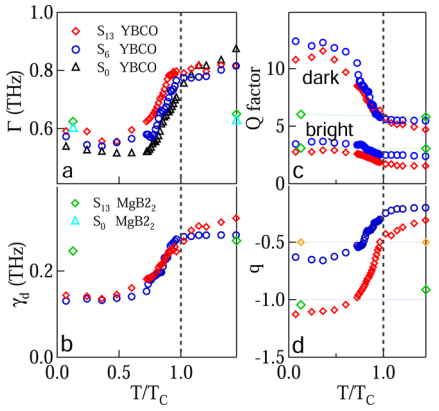


**Figure 4.** (a) Bright ($\Gamma$) and (b) dark ($\gamma_d$) damping parameters for the $S_0$ (black), $S_6$ (blue), and $S_{13}$ (red) YBCO and $S_0$ (light blue) and $S_{13}$ (green) MgB2 samples vs $T/T_c$. (c) Quality factors for the bright (bottom) and dark (top) mode for samples exhibiting EIT. (d) Fano asymmetry factor $q$ for $S_6$ and $S_{13}$ modulated by temperature. The values at the highest and lowest $T$ are reported also for MgB2 samples (showing no modulation with $T$). Dashed vertical line indicates critical temperature where $T/T_c$ = 1 for each superconductor.

almost a factor of 2 when YBCO undergoes the superconducting transition, due to the reduction of ohmic losses. When cooling at $T < T_c$, $\Gamma$ decreases from a value of about 0.8 THz to a residual damping of nearly 0.5 THz. This indicates that ohmic losses in the superconducting state are negligible (although not absent in YBCO at 1.8 THz), and we can therefore ascribe the residual damping to radiative decay.

The dark mode damping, $\gamma_d$, reported in Figure 4b is independent of the sample geometry. Therefore, the reduction of the imaginary part of the THz dielectric function in the superconducting phase results in a strong suppression of losses, and $\gamma_d$ reaches a value of ∼0.15 THz. This residual damping may have a radiative nature due to the weak coupling of the quadrupolar mode to incident radiation: this is allowed by the slight symmetry breaking introduced by the horizontal arm S.[16]

One can observe that while the dark mode is mainly affected by ohmic loss, both ohmic dissipation and radiative interaction enter in the bright-mode damping factor. Although the radiative damping depends on the distance among resonators (i.e., the amount of metallic materials in the unit cell), in our case the $x,y$ pitches are constant and the unique variation from $S_0$ to $S_{13}$ is related to the horizontal arm S, which varies from 0 to 13.5 $\mu$m. Thus, we can assume that the radiative damping is practically independent of S and constant for all resonators.

The quality factors $Q$ have been calculated for both the bright ($\omega_b/\Gamma$) and dark ($\omega_d/\gamma_d$) modes and are reported in Figure 4c. For the bright mode, $Q$ varies in the range 1−4, which are typical values encountered in the literature for planar dipole antenna arrays at THz frequencies: ohmic losses suppression in the superconducting phase is moderate and does not provide a remarkable improvement in the device performance. On the contrary, the dark mode $Q$ is improved by a factor of 3 when crossing the superconducting transition, reaching a value at low $T$ of 13. The Fano asymmetry parameters are reported in Figure 4d and are found to be $q$ = −0.6 and $q$ = −1.1 for the $S_6$ and $S_{13}$ sample, respectively, at $T < T_c$. A negative value is expected from the condition $\omega_a < \omega_b$,[19]


dx.doi.org/10.1021/ph500104k | ACS Photonics 2014, 1, 570−575

and the absolute value close to 1 for the $S_{13}$ sample indicates that the maximum possible interaction strength has been reached with this geometry. In order to quantitatively evaluate the tuning advantages of YBCO EIT, we have also extracted the resonance parameters for $MgB_2$ $S_{13}$ and $S_0$ samples (reported in green/light blue in Figure 4). It is straightforward to note that both the damping mechanisms (and consequently EIT modulation) are not affected by a temperature change of more than 1 order of magnitude.

## CONCLUSION

In this paper we have presented a proof-of-concept experiment for inducing and tuning a plasmonic analogue of electromagnetically induced transparency through superconductivity in THz plasmonic devices. The electromagnetic transparency is engineered in terms of a near-field interaction between a bright and a dark mode within a unit cell with an increasing degree of geometric asymmetry. The transparency window can be tuned by modulating the superconducting state of a high-$T_c$ YBCO superconductor through temperature. In this way, one achieves a maximum relative tuning of about 50% of the transparency window at 1.8 THz upon varying the temperature by a few degrees across $T_c$ = 85 K, i.e., above the liquid nitrogen temperature. This tuning is determined by the combination of ohmic damping suppression enabled by superconductivity and radiative damping reduction of the dark (subradiant) quadrupolar mode modulating the transparency window. The resulting device quality factor reaches a value of 13, exceeding the standard values in THz metamaterials by a factor of 5. These results are strongly promising for high quality factor terahertz optical modulators based on high-$T_c$ superconductors where optical tunability could be further obtained through electric, magnetic, and current external excitations.

## ASSOCIATED CONTENT

### Supporting Information

This material is available free of charge via the Internet at http://pubs.acs.org.

## AUTHOR INFORMATION

### Corresponding Author

*E-mail: odeta.limaj@epfl.ch.

### Notes

The authors declare no competing financial interest.

## ACKNOWLEDGMENTS

The work at Temple was supported by ONR under Grant No. N00014-13-1-0052.

## REFERENCES

(1) Harris, S. E. Electromagnetically induced transparency. *Phys. Today* **1997**, *50*, 36−42.
(2) Hau, L. V.; Harris, S. E.; Dutton, Z.; Behroozi, C. H. Light speed reduction to 17 metres per second in an ultracold atomic gas. *Nature* **1999**, *397*, 594−598.
(3) Lukin, M. D.; Imamoglu, A. Controlling photons using electromagnetically induced transparency. *Nature* **2001**, *413*, 273−276.
(4) Liu, C.; Dutton, Z.; Behroozi, C. H.; Hau, L. V. Observation of coherent optical information storage in an atomic medium using halted light pulses. *Nature* **2001**, *409*, 490−493.
(5) Sun, Y.; Tan, W.; Liang, L.; Jiang, H.-T.; Wang, Z.-G.; Liu, F.-Q.; Chen, H. Metamaterial analog of quantum interference: from electromagnetically induced transparency to absorption. *EPL* **2012**, *98*, 64007.
(6) Liu, N.; Weiss, T.; Mesch, M.; Langguth, L.; Eigenthaler, U.; Hirscher, M.; Sonnichsen, C.; Giessen, H. Planar metamaterial analogue of electromagnetically induced transparency for plasmonic sensing. *Nano Lett.* **2010**, *10*, 1103−1107.
(7) Papasimakis, N.; Fedotov, V. A.; Zheludev, N. I.; Prosvirnin, S. L. Metamaterial analog of electromagnetically induced transparency. *Phys. Rev. Lett.* **2008**, *101*, 253903.
(8) Artar, A.; Yanik, A. A.; Altug, H. Multispectral plasmon induced transparency in coupled meta-atoms. *Nano Lett.* **2011**, *11*, 1685−1689.
(9) Yanik, M. F.; Suh, W.; Wang, Z.; Fan, S. Stopping light in a waveguide with an all-optical analog of electromagnetically induced transparency. *Phys. Rev. Lett.* **2004**, *93*, 233903.
(10) Zhang, S.; Genov, D. A.; Wang, Y.; Liu, M.; Zhang, X. Plasmon-induced transparency in metamaterials. *Phys. Rev. Lett.* **2008**, *101*, 047401.
(11) Xu, Q.; Sandhu, S.; Povinelli, M. L.; Shakya, J.; Fan, S.; Lipson, M. Experimental realization of an on-chip all-optical analogue to electromagnetically induced transparency. *Phys. Rev. Lett.* **2006**, *96*, 123901.
(12) Gu, J.; Singh, R.; Liu, X.; Zhang, X.; Ma, Y.; Zhang, S.; Maier, S. A.; Tian, Z.; Azad, A. K.; Chen, H.-T.; Taylor, A. J.; Han, J.; Zhang, W. Active control of electromagnetically induced transparency analogue in terahertz metamaterials. *Nat. Commun.* **2012**, *3*, 1151.
(13) Pryce, I. M.; Aydin, K.; Kelaita, Y. A.; Briggs, R. M.; Atwater, H. A. Highly strained compliant optical metamaterials with large frequency tunability. *Nano Lett.* **2010**, *10*, 4222−4227.
(14) Fedotov, V. A.; Tsiatmas, A.; Shi, J. H.; Buckingham, R.; de Groot, P.; Chen, Y.; Wang, S.; Zheludev, N. I. Temperature control of Fano resonances and transmission in superconducting metamaterials. *Opt. Express* **2010**, *18*, 9015−9019.
(15) Kurter, C.; Tassin, P.; Zhang, L.; Koschny, T.; Zhuravel, A. P.; Ustinov, A. V.; Anlage, S. M.; Soukoulis, C. M. Classical analogue of electromagnetically induced transparency with a metal-superconductor hybrid metamaterial. *Phys. Rev. Lett.* **2011**, *107*, 043901.
(16) Wu, C.; Khanikaev, A. B.; Adato, R.; Arju, N.; Yanik, A. A.; Altug, H.; Shvets, G. Fano-resonant asymmetric metamaterials for ultrasensitive spectroscopy and identification of molecular monolayers. *Nat. Mater.* **2012**, *11*, 69−75.
(17) Dong, Z.-G.; Liu, H.; Cao, J.-X.; Li, T.; Wang, S.-M.; Zhu, S.-N.; Zhang, X. Enhanced sensing performance by the plasmonic analog of electromagnetically induced transparency in active metamaterials. *Appl. Phys. Lett.* **2010**, *97*, 114101.
(18) Lassiter, J. B.; Sobhani, H.; Knight, M. W.; Mielczarek, W. S.; Nordlander, P.; Halas, N. J. Designing and deconstructing the Fano lineshape in plasmonic nanoclusters. *Nano Lett.* **2012**, *12*, 1058−1062.
(19) Giannini, V.; Francescato, Y.; Amrania, H.; Phillips, C. C.; Maier, S. A. Fano resonances in nanoscale plasmonic systems: a parameter-free modeling approach. *Nano Lett.* **2011**, *11*, 2835−2840.
(20) Limaj, O.; D'Apuzzo, F.; Di Gaspare, A.; Giliberti, V.; Domenici, F.; Sennato, S.; Bordi, F.; Lupi, S.; Ortolani, M. Mid-infrared surface plasmon polariton sensors resonant with the vibrational modes of phospholipid layers. *J. Phys. Chem. C* **2013**, *117*, 19119−19126.
(21) Limaj, O.; Ortolani, M.; Giliberti, V.; Di Gaspare, A.; Mattioli, F.; Lupi, S. Field distribution and quality factor of surface plasmon resonances of metal meshes for mid-infrared sensing. *Plasmonics* **2013**, *8*, 851−858.
(22) Di Pietro, P.; Ortolani, M.; Limaj, O.; Di Gaspare, A.; Giliberti, V.; Giorgianni, F.; Brahlek, M.; Bansal, N.; Koirala, N.; Oh, S.; Calvani, P.; Lupi, S. Observation of Dirac plasmons in a topological insulator. *Nat. Nanotechnol.* **2013**, *8*, 556−560.
(23) Chen, H.-T.; Yang, H.; Singh, R.; O'Hara, J. F.; Azad, A. K.; Trugman, S. A.; Jia, Q. X.; Taylor, A. J. Tuning the resonance in high-temperature superconducting terahertz metamaterials. *Phys. Rev. Lett.* **2010**, *105*, 247402.
(24) Jin, B. B.; Zhang, C. H.; Engelbrecht, S.; Pimenov, A.; Wu, J. B.; Xu, Q. Y.; Cao, C. H.; Chen, J.; Xu, W. W.; Kang, L.; Wu, P. H. Low

loss and magnetic field-tunable superconducting terahertz metamaterial. *Opt. Express* **2010**, *18*, 17504−17509.
(25) Wu, J.; Jin, B.; Xue, Y.; Zhang, C.; Dai, H.; Zhang, L.; Cao, C.; Kang, L.; Xu, W.; Chen, J.; Wu, P. Tuning of superconducting niobium nitride terahertz metamaterials. *Opt. Exp.* **2011**, *19*, 12021−12026.
(26) Anlage, S. M. The physics and applications of superconducting metamaterials. *J. Opt.* **2011**, *13*, 024001.
(27) Kurter, C.; Abrahams, J.; Shvets, G.; Anlage, S. M. Plasmonic scaling of superconducting metamaterials. *Phys. Rev. B* **2013**, *88*, 180510 (R).
(28) Pryce, I. M.; Kelaita, Y. A.; Aydin, K.; Atwater, H. A. Compliant metamaterials for resonantly enhanced infrared absorption spectroscopy and refractive index sensing. *ACS Nano* **2011**, *5*, 8167−8174.
(29) Adato, R.; Artar, A.; Erramilli, S.; Altug, H. Engineered absorption enhancement and induced transparency in coupled molecular and plasmonic resonator systems. *Nano Lett.* **2013**, *13*, 2583−2591.
(30) Ricci, M.; Orloff, N.; Anlage, S. M. Superconducting metamaterials. *Appl. Phys. Lett.* **2005**, *87*, 034102.
(31) Gu, J.; Singh, R.; Tian, Z.; Cao, W.; Xing, Q.; He, M.; Zhang, J. W.; Han, J.; Chen, H. T.; Zhang, W. Terahertz superconductor metamaterial. *Appl. Phys. Lett.* **2010**, *97*, 071102.
(32) Puchkov, A. V.; Basov, D. N.; Timusk, T. The pseudogap state in high-Tc superconductors: an infrared study. *J. Phys.: Condens. Matter* **1996**, *8*, 10049−10082.
(33) Lobo, R. P. S. M.; Bontemps, N.; Racah, D.; Dagan, Y.; Deutscher, G. Pseudo-gap and superconducting condensate energies in the infrared spectra of Pr-doped $YBa_2Cu_3O_7$. *Europhys. Lett.* **2001**, *55*, 854−860.
(34) Chen, M. *Optical studies of high temperature superconductors and electronic dielectric materials*. Ph.D. Thesis, University of Florida, 2005.
(35) Kaindl, R. A.; Carnahan, M. A.; Orenstein, J.; Chemla, D. S.; Christen, H. M.; Zhai, H.; Paranthaman, M.; Lowndes, D. H. Far-infrared optical conductivity gap in superconducting MgB2 films. *Phys. Rev. Lett.* **2001**, *88*, 027003.
(36) Fang, X.; Zhuang, C.; Wen, Z.; Han, X.; Feng, Q.; Xi, X. X.; Nori, F.; Xie, X.; Niu, Q.; Qiu, X. Influence of intrinsic electronic properties on light transmission through subwavelength holes on gold and MgB2 thin films. *Phys. Rev. B* **2011**, *84*, 205438.
(37) Ortolani, M.; Dore, P.; Di Castro, D.; Perucchi, A.; Lupi, S.; Ferrando, V.; Putti, M.; Pallecchi, I.; Ferdeghini, C.; Xi, X. X. Two-band parallel conductivity at terahertz frequencies in the superconducting state of MgB2. *Phys. Rev. B* **2008**, *77*, 100507(R).
(38) Ortolani, M.; Di Castro, D.; Postorino, P.; Pallecchi, I.; Monni, M.; Putti, M.; Dore, P. Clean and dirty superconductivity in pure, Al doped, and neutron irradiated MgB2: a far-Infrared study. *Phys. Rev. B* **2005**, *71*, 172508.
(39) Brubach, J. B.; Manceron, L.; Rouzieres, M.; Pirali, O.; Balcon, D.; Kwabia Tchana, F.; Boudon, V.; Tudorie, M.; Huet, T.; Cuisset, A.; Roy, P. Performance of the AILES THz-infrared beamline at SOLEIL for high resolution spectroscopy. *AIP Conf. Proc.* **2010**, *1214*, 81−84.
(40) Roy, P.; Cestelli Guidi, M.; Nucara, A.; Marcouille, O.; Calvani, P.; Giura, P.; Paolone, A.; Mathis, Y.-L.; Gerschel, A. Spectral distribution of infrared synchrotron radiation by an insertion device and its edges: a comparison between experimental and simulated spectra. *Phys. Rev. Lett.* **2000**, *84*, 483−486.
(41) Francescato, Y.; Giannini, V.; Maier, S. A. Plasmonic systems unveiled by Fano resonances. *ACS Nano* **2012**, *6*, 1830−1838.
(42) Rahmani, M.; Lukyanchuk, B.; Hong, M. Fano resonance in novel plasmonic nanostructures. *Laser Photonics Rev.* **2012**, *7*, 1−21.
(43) Balanis, C. A. *Modern Antenna Handbook*; John Wiley & Sons: New York, 2011; p 2.3..
(44) Encina, E. R.; Coronado, E. A. Plasmonic nanoantennas: angular scattering properties of multipole resonances in noble metal nanorods. *J. Phys. Chem. C* **2008**, *112*, 9586−9594.
(45) Gallinet, B.; Martin, O. J. F. Influence of electromagnetic interactions on the line shape of plasmonic Fano resonances. *ACS Nano* **2011**, *5*, 8999−9008.
(46) Gallinet, B.; Martin, O. J. F. Ab initio theory of Fano resonances in plasmonic nanostructures and metamaterials. *Phys. Rev. B* **2011**, *83*, 235427.